Introduction to Pump Rotordynamics

Luis San Andrés
Mast-Childs Tribology Professor
Turbomachinery Laboratory
Texas A&M University
College Station, TX 77843-3123
USA

Lsanandres@mengr.tamu.edu

ABSTRACT

The lecture introduces the basic problems in the rotordynamics of turbomachinery, excessive vibration and instability. The acceptable performance of a turbomachine depends on the adequate design and operation of the bearing and seal elements supporting a rotor. Descriptions of the basic principles of lubrication follow with details on the operation of hydrodynamic and hydrostatic lubricated bearings and seals. The differences among these elements are highlighted with a brief account on their effects on rotordynamics. The basic equations for the modeling of linear rotor-bearing systems are given along with an example for the rotordynamics of a multiple stage compressor. Pump rotordynamics is introduced noting the major difference with other rotating systems, i.e. hydraulic side loads, static and dynamic, due to pressure changes in the volute and flow conditions in an impeller, dynamic forces from seals – neck ring and interstage and balance pistons, and impeller-rotor interaction forces. Accounting for the action of these elements is of importance to adequately predict the performance and troubleshoot the rotordynamics of high performance pumps. An example of rotordynamic analysis of a multiple-stage liquid pump stresses the differences between "wet' and "dry" predictions, i.e. operation with and without the pumping liquid.

1.0 INTRODUCTION

A turbomachinery is a rotating structure where the load or the driver handles a process fluid from which power is extracted or delivered to. Examples of turbomachines include pumps and compressors, gas and steam turbines, turbo generators and turbo expanders, turbochargers, APU (auxiliary power units), etc.

Most turbomachinery is supported on oil lubricated fluid film bearings, although modern advances and environmental restrictions are pushing towards the implementation of process fluid bearings and even gas bearing applications. Fluid film bearings are used due to their adequate load support, good damping characteristics and absence of wear if properly designed and operated.

Turbomachines also include a number of other mechanical elements which provide stiffness and damping characteristics and affect the dynamics of the rotor-bearing system. Impeller seals, floating ring seals, thrust collars and balance pistons are a few of these elements.

The adequate operation of a turbomachine is defined by its ability to tolerate normal (and even abnormal) vibrations levels without affecting significantly its overall performance (reliability and efficiency).

The rotordynamics of turbomachinery encompasses the structural analysis of rotors (shafts and disks) and the design of fluid film bearings and seals that determine the best dynamic performance given the required

San Andrés, L. (2006) Introduction to Pump Rotordynamics. In *Design and Analysis of High Speed Pumps* (pp. 9-1 – 9-26). Educational Notes RTO-EN-AVT-143, Paper 9. Neuilly-sur-Seine, France: RTO. Available from: http://www.rto.nato.int/abstracts.asp.

operating conditions. This best performance is denoted by well-characterized natural frequencies (and critical speeds) with amplitudes of synchronous dynamic response within required standards and demonstrated absence of subsynchronous vibration instabilities.

A rotordynamic analysis considers the interaction between the elastic and inertia properties of the rotor and the mechanical impedances from the fluid film bearing supports, oil seal rings, seals, etc.

The **most commonly recurring problems in rotordynamics** are [1]

1. Excessive steady state synchronous vibration levels.
2. Sub harmonic rotor instabilities.

Steady state vibration levels may be reduced by:

a) Improving balancing.
b) Modifying rotor-bearing systems: tune system critical speeds out of RPM operating range.
c) Introducing damping to limit peak amplitudes at critical speeds that must be traversed.

Sub harmonic rotor instabilities may be avoided by:

a) Raising the natural frequency of rotor system as much as possible.
b) Eliminating the instability mechanism, i.e. change bearing design if oil whip is present.
c) Introducing damping to raise onset speed above the operating speed range.

Rotordynamic instabilities have become more common as the speed and power of turbomachinery increased. These instabilities can sometimes be erratic, seemingly increasing vibration amplitudes for no apparent reason. A common denominator among many stability problems is that they tend to grow with time as the affected component(s) begins to wear or fatigue.

For example, two typical destabilizing forces well documented in the technical literature are due to the aerodynamic effects of labyrinth seals and the hydrodynamic effects of lubricated cylindrical bearings and floating oil ring seals in centrifugal compressors. Load, gas molecular weight, and oil pressure and temperature are factors to generate severe problems in problematic turbomachinery.

The detailed study of rotordynamics demands accurate knowledge of the particular mechanical elements supporting the rotor, i.e. fluid film bearings and seals.

2.0 DESCRIPTIONS OF FLUID FILM BEARINGS

Fluid film bearings are machine elements designed to produce smooth (low friction) motion between solid surfaces in relative motion and to generate a load support for mechanical components. The lubricant or fluid between the surfaces may be a liquid, a gas or even a solid (coating).

Fluid film bearings, if well designed, are able to support static and dynamic loads, and consequently, their effects on the performance of rotating machinery are of great importance.

These notes focus on the analysis of bearings with a full film separating the mechanical surfaces. The word *film* implies that the fluid thickness (gap or clearance) separating the surfaces is several orders of magnitude smaller than the other dimensions of the bearing, i.e. width and length. Yet the film thickness is larger than the micro asperities in the surfaces thus warranting operation without contact of surfaces.

The basic operational principles of fluid film bearings are hydrodynamic, hydrostatic or hybrid (a combination of the former two).

2.1 Hydrodynamic or Self-Acting Fluid Film Bearings

In hydrodynamic bearings there is relative motion between two mechanical surfaces with a particular "wedge like" shape, See Figure 1. The fluid dragged into the film generates a hydrodynamic pressure field able to support an externally applied load, static and/or dynamic. In general [2]:

Advantages	Disadvantages
Do not require external source of pressure. Fluid flow is dragged into the convergent gap in the direction of the surface relative motion. Support heavy loads. The load support is a function of the lubricant viscosity, surface speed, surface area, film thickness and geometry of the bearing. Long life (infinite in theory) without wear of surfaces. Provide stiffness and damping coefficients of large magnitude.	Thermal effects affect performance if film thickness is too small or available flow rate is too low. Require of surface relative motion to generate load support. Induce large drag torque (power losses) and potential surface damage at start-up (before lift-off) and touch down. Potential to induce hydrodynamic instability, i.e. loss of effective damping for operation well above critical speed of rotor-bearing system.

2.2 Hydrostatic or Externally-Pressurized Fluid Film Bearings

In hydrostatic bearings, an external source of pressurized fluid forces the lubricant to flow between the surfaces, thus enabling their separation and the ability to support a load without surface contact, and most importantly, without relative motion. See Figure 2 for a typical geometry. In general [2]:

Advantages	Disadvantages
Support very large loads. The load support is a function of the pressure drop across the bearing and the area of fluid pressure action. Load does not depend on film thickness or lubricant viscosity. Long life (infinite in theory) without wear of surfaces Provide stiffness and damping coefficients of very large magnitude. Excellent for exact positioning and control.	Require ancillary equipment. Larger installation and maintenance costs. Need of fluid filtration equipment. Loss of performance with fluid contamination. High power consumption because of pumping losses. Potential to induce hydrodynamic instability in hybrid mode operation. Potential to show pneumatic hammer instability for highly compressible fluids, i.e. loss of damping at low and high frequencies of operation due to compliance and time lag of trapped fluid volumes.

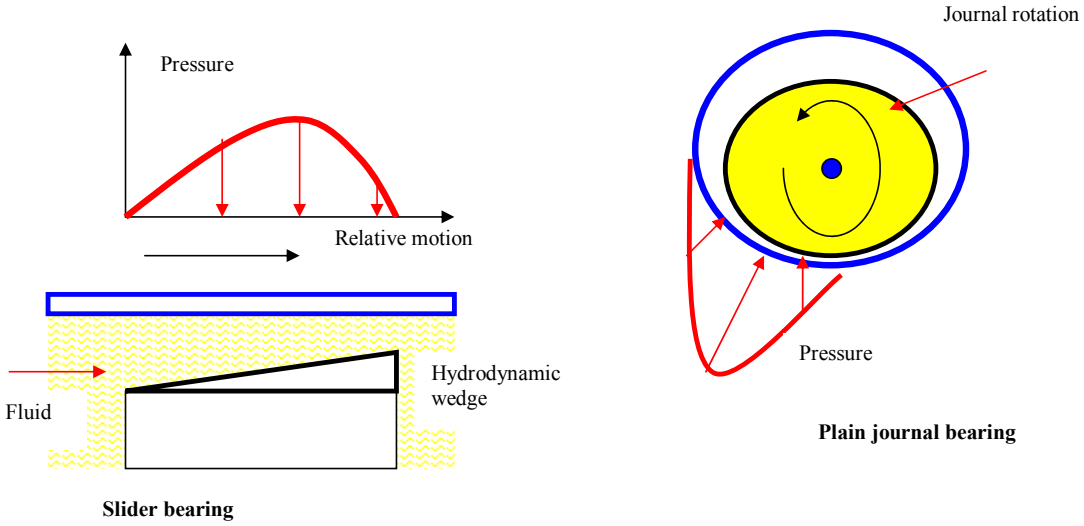

Figure 1: Schematic Views of Hydrodynamic (Self-Acting) Fluid Film Bearing.

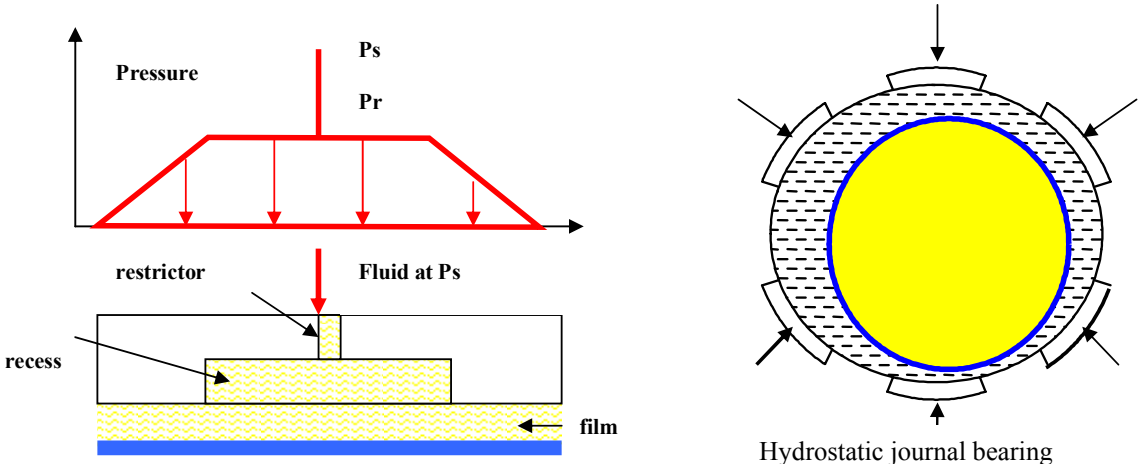

Figure 2: Schematic Views of Hydrostatic (Pressurized) Fluid Film Bearing.

Figure 3 depicts schematic views of hydrodynamic journal bearings, single and multiple lobes, and multiple pads. The cylindrical bearings feature feed ports for lubricant inlet as well as pad or lobes machined with a preload to generate a film wedge upon shaft rotation.

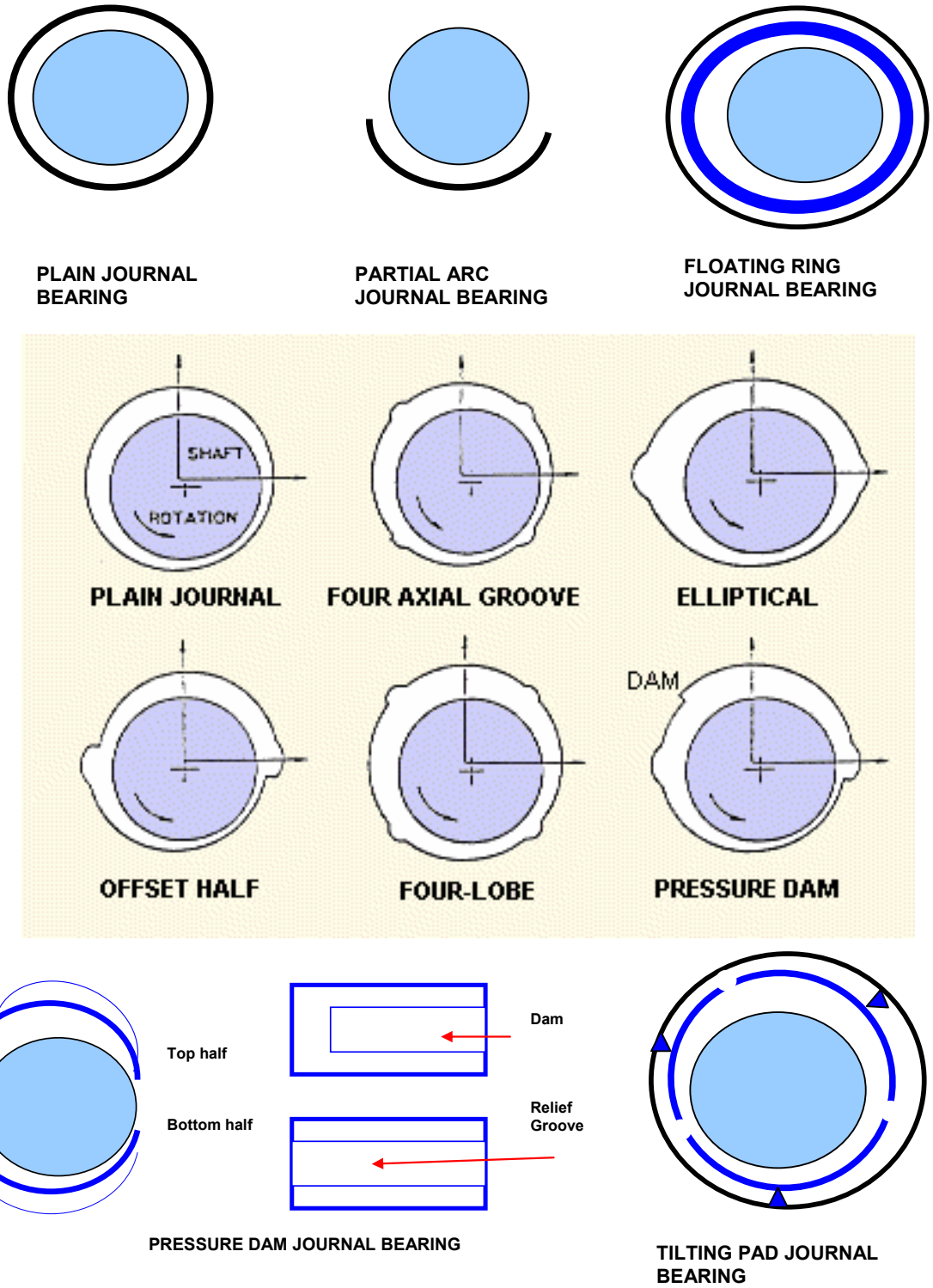

Figure 3: Schematic Views of Typical Cylindrical Journal Bearings.

2.3 Squeeze Film Dampers

Normal motions can also generate hydrodynamic pressures in the thin film separating two surfaces. This squeeze film action mechanism works effectively only for compressive loads, i.e. those forcing the approach of one surface to the other. **Squeeze film dampers** are routinely implemented to reduce

vibration amplitudes and isolate structural components in gas jet engines, high performance compressors, and occasionally in water pumps.

A squeeze film damper consists of an inner non rotating journal and a stationary outer bearing, both of nearly identical diameters. Figure 4 shows an idealized schematic of this type of fluid film bearing. A journal is mounted on the external race of a rolling element bearing and prevented from spinning with loose pins or a squirrel cage that provides a centering elastic mechanism. The annular thin film, typically less than 0.250 mm, between the journal and housing is filled with a lubricant provided as a splash from the rolling bearing elements lubrication system or by a dedicated pressurized delivery. In operation, as the journal moves due to dynamic forces acting on the system, the fluid is displaced to accommodate these motions. As a result, hydrodynamic squeeze film pressures exert reaction forces on the journal and provide for a mechanism to attenuate transmitted forces and to reduce the rotor amplitude of motion [3].

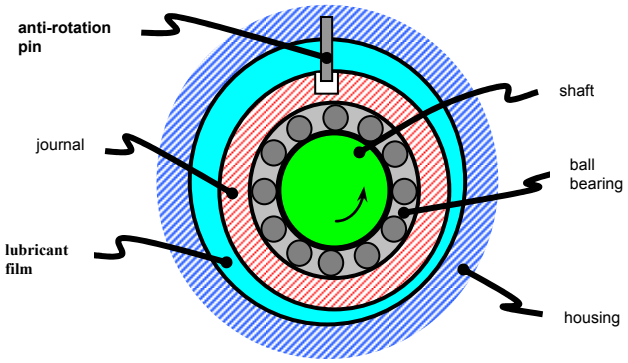

Figure 4: Typical Squeeze Film Damper Configuration.

2.4 Annular Pressure Seals

Radial seals (annular, labyrinth or honeycomb) separate regions of high pressure and low pressure in rotating machinery and their function is to minimize the leakage and improve the overall efficiency of a rotating machine extracting or delivering power to a fluid. Typical applications include neck ring seals on impeller eyes and inter stage seals as well as balance pistons in pump and compressor applications, as depicted in Figure 5. Seals have larger clearances than load carrying bearings. Yet their impact on the rotordynamics of turbomachinery is of importance since seals are located at rotor positions where large vibrations occur [4].

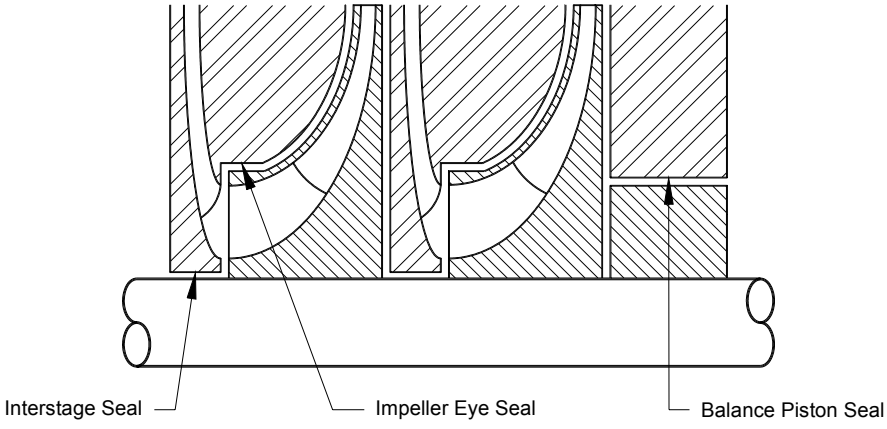

Figure 5: Seals in a Multistage Centrifugal Pump or Compressor.

Extensive testing has shown that seals with macroscopic roughness; i.e. textured stator surfaces, offer major improvements in reducing leakage as well as cross-coupled stiffness coefficients [5]. Figure 6 depicts two textured seals and a conventional labyrinth seal (teeth on stator). A textured surface like a round-hole pattern or a honeycomb increases the friction thus reducing leakage, and aids to retard the development of the circumferential flow velocity -the physical condition generating the cross-coupled stiffness coefficients. In the past 10 years, compressor and pump manufacturers, as well as users, are implementing textured seals with great commercial success [6].

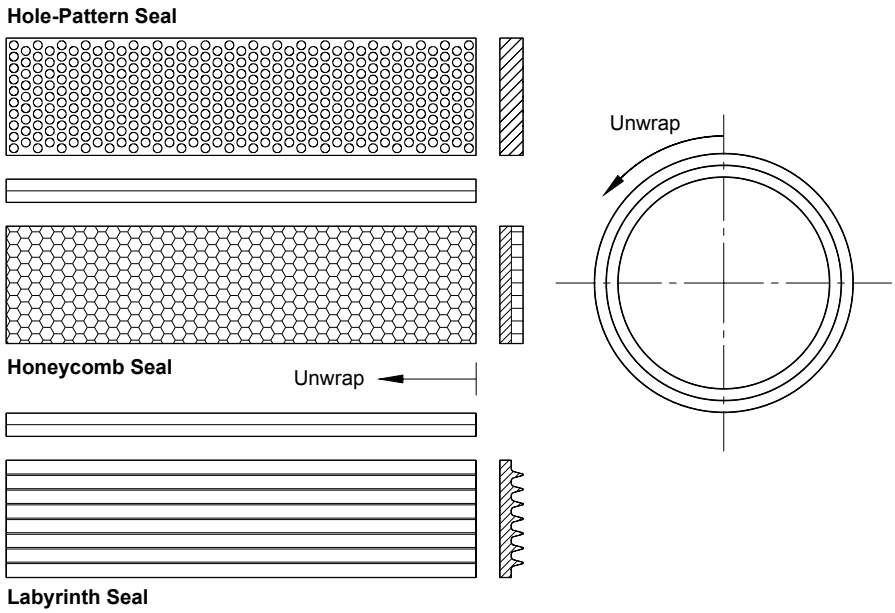

Figure 6: Hole-Pattern, Honeycomb and Labyrinth Seal Configurations.

3.0 BASICS OF A ROTORDYNAMIC ANALYSIS

The objectives of a rotordynamic analysis are:

a) To model the rotor (shaft and disks) and to determine its free-free natural frequencies.

b) To model the fluid film bearing and seal elements and to calculate the mechanical impedances (stiffness, damping and inertia force coefficients connecting the rotor to its casing).

c) To perform an eigenvalue analysis, i.e. to predict the damped natural frequencies and damping ratios for the different modes (rigid and elastic) of vibration of the rotor as the rotor speed increases to values well above its design operating conditions. Positive damping ratios evidence the absence of rotordynamic instability.

d) To perform a synchronous response analysis to calibrated imbalances in order to predict the maximum amplitudes of vibration, the safe passage through critical speeds and to estimate the loads transmitted through the bearing supports.

e) To certify the reliable performance of the rotor-bearing system satisfying established engineering criteria (API qualification) and to emit recommendations to improve the system performance (response and stability).

It is important to stress that the tasks (objectives) above need of extensive experimental and field support verification. Analysis without adequate field or shop measurements is usually not very useful in rotordynamics.

3.1 Equations of Motion for Rotor-Bearing System

The general equations for lateral motions of a rotor are [4]:

$$([M]+[N])_R\{\ddot{u}\}-\Omega[G]_R\{\dot{u}\}+[K]_R\{u\}=\{F(u,\dot{u},t)\} \tag{1}$$

where $[M]$ and $[N]$ are global translational and rotary mass matrices, $[G]$ and $[K]$ are gyroscopic and stiffness matrices, Ω is the rotor speed, $\{u\}$ represent the rotor displacements (translations and rotations), and $\{F(u,\dot{u},t)\}$ denote bearing and seal reaction forces and the distributed imbalance vector, for example, The in-house finite element rotordynamics code[7] is based on Timoshenko beam theory [8] and implements component-mode synthesis [9] to model multiple shaft rotors. The program interfaces with a number of bearing and seal codes also developed in-house.

3.2 Representations of Bearing and Seal Forces

In a linear lateral rotordynamics model, bearing and seal reaction forces are linear functions of the rotor motion. Bearing dynamic forces along directions (X, Y) perpendicular to the rotor spin axis (Z) are represented in terms of force coefficients (See Figure 7), i.e.

$$\begin{bmatrix} F_X \\ F_Y \end{bmatrix} = -\begin{bmatrix} K_{XX} & K_{XY} \\ K_{YX} & K_{YY} \end{bmatrix}_B \begin{Bmatrix} X \\ Y \end{Bmatrix} - \begin{bmatrix} C_{XX} & C_{XY} \\ C_{YX} & C_{YY} \end{bmatrix}_B \begin{Bmatrix} \dot{X} \\ \dot{Y} \end{Bmatrix} \tag{2}$$

where $[K]_B$ and $[C]_B$ denote matrices of stiffness and damping force coefficients. The force coefficients are strictly valid for small amplitude motions or perturbations about an equilibrium condition. The static load acting on each bearing and shaft speed determine the equilibrium state. Force coefficients for oil-lubricated bearings are frequency independent parameters, though changing with the operating shaft speed and load condition. Fluid film bearings handling compressible liquids and gases generate frequency dependent force coefficients.

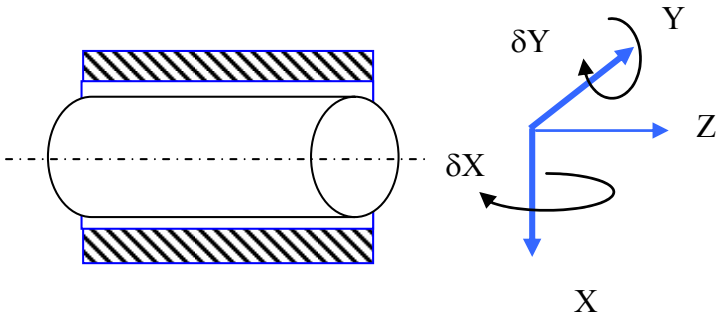

Figure 7: DOF Lateral Displacements (X,Y) and Angulations (δX, δY).

The representation of liquid seal forces for lateral motions (X, Y) is given as [4]

$$\begin{bmatrix} F_X \\ F_Y \end{bmatrix} = -\begin{bmatrix} K_{XX} & K_{XY} \\ K_{YX} & K_{YY} \end{bmatrix}_S \begin{Bmatrix} X \\ Y \end{Bmatrix} - \begin{bmatrix} C_{XX} & C_{XY} \\ C_{YX} & C_{YY} \end{bmatrix}_S \begin{Bmatrix} \dot{X} \\ \dot{Y} \end{Bmatrix} - \begin{bmatrix} M_{XX} & M_{XY} \\ M_{YX} & M_{YY} \end{bmatrix}_S \begin{Bmatrix} \ddot{X} \\ \ddot{Y} \end{Bmatrix} \tag{3}$$

where $[K]_S$, $[C]_S$ and $[M]_S$ represent matrices of stiffness, damping and inertia force coefficients. Added mass coefficients are of importance in liquid seals due to the large density of the fluid pumped.

Dynamic reaction forces in gas seals are nowadays represented as

$$\begin{bmatrix} F_X \\ F_Y \end{bmatrix} = -\begin{bmatrix} K_{XX}(\omega) & K_{XY}(\omega) \\ K_{YX}(\omega) & K_{YY}(\omega) \end{bmatrix}_S \begin{Bmatrix} X \\ Y \end{Bmatrix} - \begin{bmatrix} C_{XX}(\omega) & C_{XY}(\omega) \\ C_{YX}(\omega) & C_{YY}(\omega) \end{bmatrix}_S \begin{Bmatrix} \dot{X} \\ \dot{Y} \end{Bmatrix} \tag{4}$$

with force coefficients showing a complicated dependency on frequency [5].

Balance pistons are represented as long seals, and thus these elements can also generate bending moments ($M_{X,Y}$) due to lateral displacements, as well as reaction forces due to dynamic angulations (φ_X, φ_Y) around the (X, Y) axes, i.e. [4]

$$\begin{bmatrix} F_X \\ F_Y \\ M_X \\ M_Y \end{bmatrix} = -\begin{bmatrix} K_{XX} & K_{XY} & K_{X\delta X} & K_{X\delta Y} \\ K_{YX} & K_{XX} & K_{X\delta Y} & K_{X\delta X} \\ K_{\delta XX} & K_{\delta XY} & K_{\delta X\delta X} & K_{\delta X\delta Y} \\ -K_{\delta XY} & K_{\delta XX} & K_{\delta X\delta Y} & K_{\delta X\delta X} \end{bmatrix} \begin{bmatrix} X \\ Y \\ \phi_X \\ \phi_Y \end{bmatrix} - \begin{bmatrix} C_{XX} & C_{XY} & C_{X\delta X} & C_{X\delta Y} \\ C_{YX} & C_{XX} & C_{X\delta Y} & C_{X\delta X} \\ C_{\delta XX} & C_{\delta XY} & C_{\delta X\delta X} & C_{\delta X\delta Y} \\ C_{\delta XY} & C_{\delta XX} & C_{\delta X\delta Y} & C_{\delta X\delta X} \end{bmatrix} \begin{bmatrix} \dot{X} \\ \dot{Y} \\ \dot{\phi}_X \\ \dot{\phi}_Y \end{bmatrix} - \begin{bmatrix} M_{XX} & M_{XY} & M_{X\delta X} & M_{X\delta Y} \\ M_{YX} & M_{XX} & M_{X\delta Y} & M_{X\delta X} \\ M_{\delta XX} & M_{\delta XY} & M_{\delta X\delta X} & M_{\delta X\delta Y} \\ M_{\delta XY} & M_{\delta XX} & M_{\delta X\delta Y} & M_{\delta X\delta X} \end{bmatrix} \begin{bmatrix} \ddot{X} \\ \ddot{Y} \\ \ddot{\phi}_X \\ \ddot{\phi}_Y \end{bmatrix} \tag{5}$$

Incidentally, aerodynamic (or hydraulic) forces from impeller interactions in centrifugal compressors (or pumps) and axial flow turbines are also represented in a similar form.

Forces and moments from support bearings and seal force coefficients are integrated into the equations of motion (1) rendering

$$[M]\{\ddot{u}\} - [[C] - \Omega[G]_R]\{\dot{u}\} + [K]\{u\} = \{F_{ext}(u, \dot{u}, t)\} \tag{6}$$

where

$$\begin{aligned} [M] &= ([M] + [N])_R \cup \sum [M]_S; \\ [K] &= [K]_R \cup \sum [K]_B \cup \sum [K]_S; \\ [C] &= \cup \sum [C]_B \cup \sum [C]_S; \end{aligned} \tag{7}$$

are the system inertia, stiffness and damping matrices. Above sub-indices B and S represent the contributions of bearing and seals.

To determine the damped natural frequencies of the rotor-bearing system, the homogeneous form of Eqn. (6) is solved. The general solution is of the form, $\{u\} = \{v\}\, e^{st}$ which renders the following eigenvalue problem.

$$[[K] + s[C] - \Omega s[G]_R + s^2[M]]\{v\} = \{0\} \tag{8}$$

Solution of the characteristic equation (8), a polynomial in s, leads to the set of eigenvalues $s = \lambda + i\,\omega$ and eigenvectors $\{v\}$, also known as natural damped mode shapes. Note that the system eigenvalues are rotor speed dependent (Ω). For stability, the real part of all eigenvalues must be negative, i.e. $\lambda < 0$.

For synchronous response to imbalance, the vector forcing function is periodic and proportional to rotor speed, Ω^2. Letting $\{F_{ext}\} = \{m\, x\, u\, e^{i\varphi}\}\, \Omega^2\, e^{i\Omega t}$, the system response, $\{u\} = \{w\}\, e^{i\Omega t}$ is obtained by solution of the complex algebraic equation

$$[[K] + i\Omega[C] - i\Omega^2[G]_R - \Omega^2[M]]\{w\} = \{m\, x\, u\, e^{i\phi}\} \tag{9}$$

A nonlinear rotordynamics analysis does not rely on linearized bearing and seal force coefficients. For example, bearing reaction forces are expressed as general impedance formulas, $F_\alpha = f_\alpha\left(X, Y, \dot{X}, \dot{Y}\right)$, $_{\alpha=X,Y}$ that are evaluated at each time step in a transient response analysis to specific events such as machinery start-up, blade loss simulations, etc. Current (personal) computer technology with extremely fast processors has enabled the routine implementation of nonlinear models in an efficient manner. Refer to [10] for details on the development of a virtual tool for turbocharger nonlinear rotordynamics that has reduced by 70% cycle time in the development of new rotor-bearing systems.

4.0 EXAMPLE OF A ROTORDYNAMIC ANALYSIS

The brief description below details the steps and results of a rotordynamic analysis performed on a seven-stage compressor handling a light hydrocarbon mixture, see Figure 8.

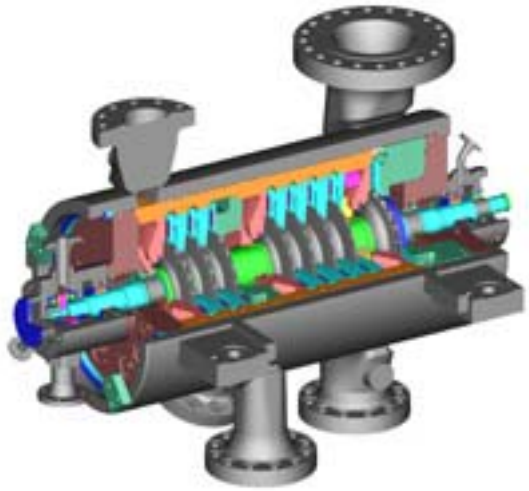

Figure 8: Cut-Away View of a Centrifugal Compressor.

Note that the typical rotordynamic analysis is linear, i.e. it relies on the representation of the bearings and seals as linear mechanical elements. That is, the second order differential equations describing the motion about an equilibrium position are linear. Of course a nonlinear analysis could also be performed but its cost could be prohibitive. In short, a linear analysis is mandatory to determine the operability of the turbomachine.

The example intends to show the complexity of a typical analysis. Figure 9 depicts the structural model with the rotor partitioned into 36 finite elements (each with inertia and elastic properties). The circles denote added inertias such as those from the impellers and thrust collars. The spring-like connections to ground represent the bearing and seal elements supporting the rotor. The tables below show the physical properties of the rotor, the compressor operating conditions (current and desired), and a brief description of the bearings and seals in place.

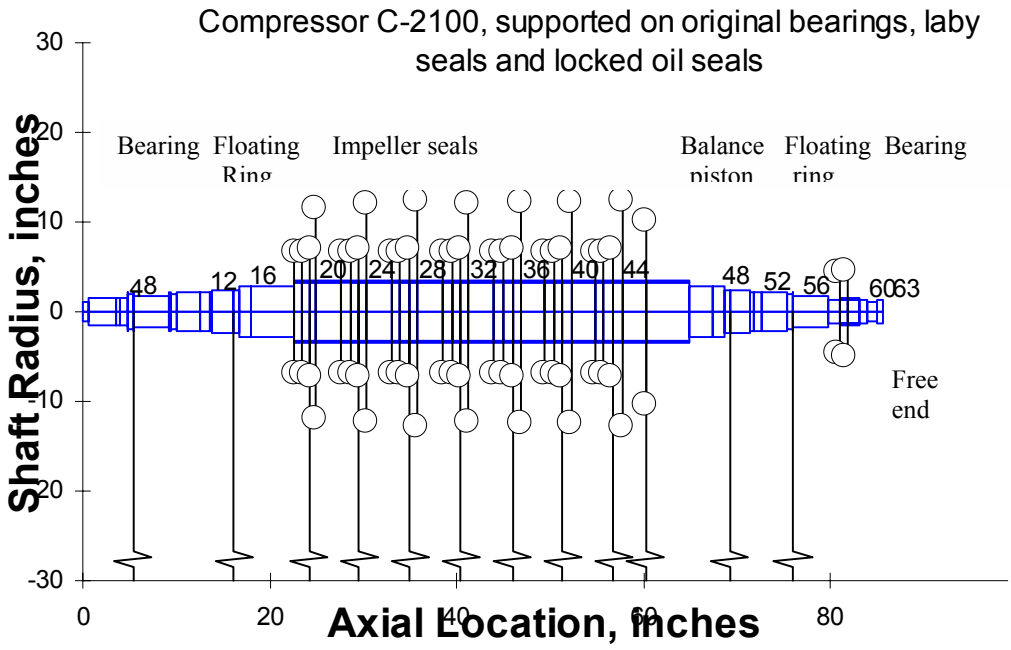

Figure 9: Finite Element Representation of Centrifugal Compressor.

Table 1: Geometry of Rotor for Compressor

Compressor C-2100	Physical units
Number of impellers	7
Shaft length	85.6 “ (2.17 m)
Rotor weight includes thrust collar	1,024 lb (4,550 N)
Center of mass from coupling side	43.65 “ – station 34
Mass moment of inertia (transversal)	302,815 lbm-in^2
Mass moment of inertia (polar)	16,749 lbm-in^2
Static load on bearing (coupling side)	469 lb (2,085 N)
Static load on bearing (free end)	554 lb (2,465 N)

Table 2: Compressor Operating Conditions
(Actual and Desired Hydrocarbon Mixture (Molecular Weight 8.72))

	5,700 RPM		**9,850 RPM**	
Stage	Pressure (bar)	Temperature (K)	Pressure (bar)	Temperature (K)
0	20.00	311.0	21.00	311
7	27.00	338.0	33.00	360

Table 3 shows the location of the mechanical impedances to ground. The rotor is supported on two multiple lobe cylindrical bearings operating with ISO VG 32 oil. Furthermore, pressurized floating oil seal rings isolate the process gas from the environment. There are also seven eye impeller seals and six inter stage seals of the labyrinth type. A long balance piston is placed at the free end of the compressor.

Table 3: Bearing and Seal Locations on Compressor

Station	Mechanical Element	Description
8	Hydrodynamic bearing	Three lobe bearing (coupling end)
56	Hydrodynamic bearing	Three lobe bearing (free end)
15	Floating ring seal	Pressurized, lubricant
50	Floating ring seal	Pressurized, lubricant
46	Balance piston	Process Gas, 27 teeth
20, 24, 28 32, 36, 40	Impeller seals – neck ring (eye) and inter stage	Labyrinth type, process gas 4 teeth
44	Eye Impeller # 7 seal	Labyrinth type, process gas

The structural finite element analysis predicts well the free-free mode natural frequency of the rotor, as shown in Table 4. The free-free mode is the first elastic mode without any connections to ground, i.e. no bearings or seals. The good correlation with the field measurement is encouraging. The field test usually consists of hanging the rotor from long cables and then raping the shaft with a heavy objects and then recording the natural frequency (and mode shape) of motion.

Table 4: Free-Free Mode Natural Frequency of Rotor (No Thrust Collar)

C-2100	Calculated	Field Measurement
Fundamental frequency	**14,431 RPM** (240 Hz)	**14,400 RPM**
2nd frequency	27,081 RPM	Unknown
3rd frequency	40,927 RPM	‘’

The linear rotordynamic analysis predicts the eigenvalues (damped natural frequencies) of the rotor operating on its bearings and seals for speeds to 20,000 rpm, twice the design value. The predictions show a lightly damped critical speed at 4,000 rpm. And most importantly, it shows rotordynamic instability at 8,163 rpm. The field measurements evidence of the subsynchronous vibration at a lower speed, i.e. 7.850 rpm!

Table 5: Threshold Speed of Instability

	Threshold Speed	Whirl Frequency	Whirl Ratio	Mode
Predicted	8,163 rpm	4,000 rpm	0.49	Elastic
Field data	7,850 rpm	3,532 rpm	0.45	mode

The top graph on Figure 10 presents the predicted damper natural frequencies versus shaft speed, with the synchronous speed line (1X) showing the location of the first critical speed at ~ 4,000 rpm. The bottom graph shows the damping ratio versus natural frequency for the various rotor modes. Note that a damping ratio less than zero denotes an instability.

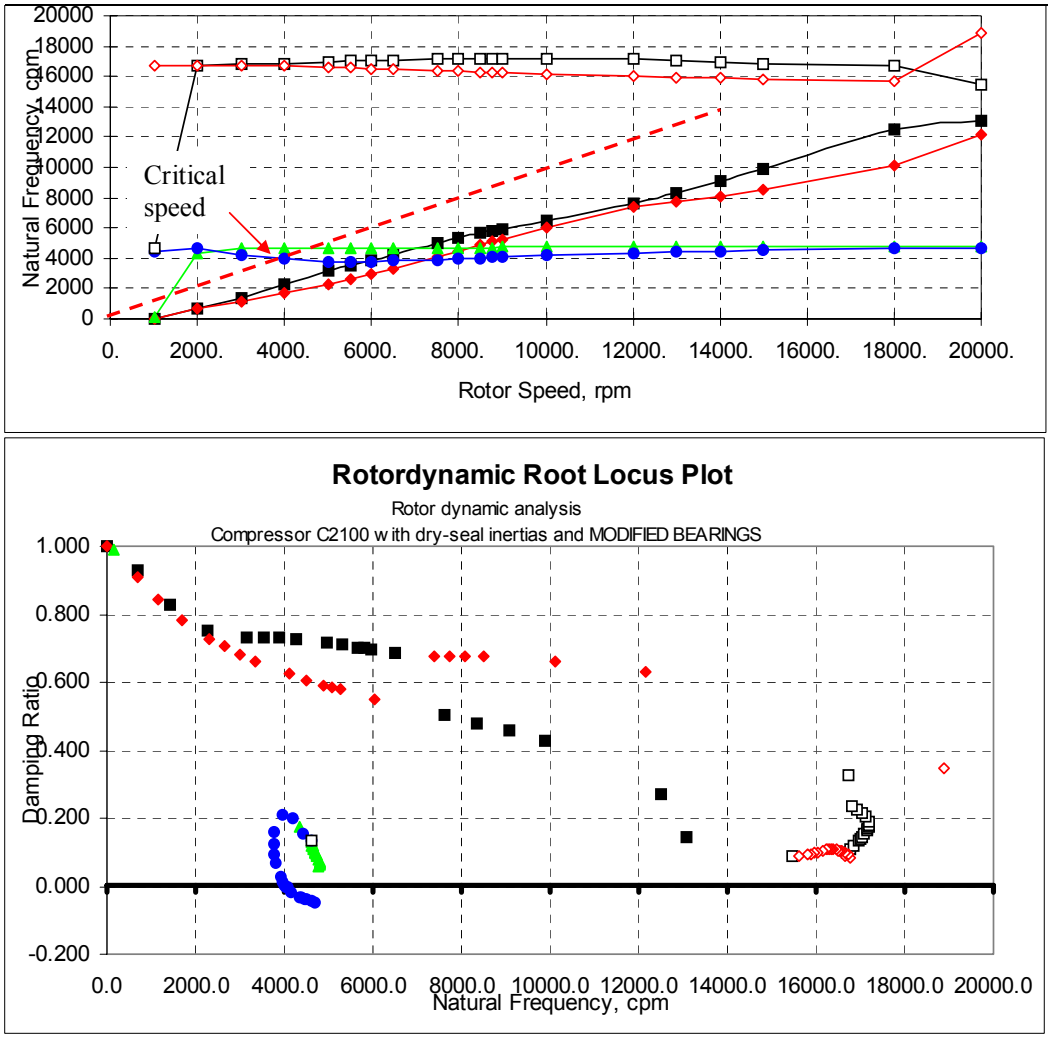

Figure 10: Damped Natural Frequencies and Damping Ratios for Example Rotor-Bearing System.

The imbalance response shown in Figure 11 depicts the amplitude of synchronous motions versus rotor speed and the mode of vibration at a rotor speed of 8,750 rpm. The predictions are not valid for operating speeds above the threshold speed of instability since the rotor vibrates with a subsynchronous frequency of amplitude much larger than the one synchronous with rotor speed.

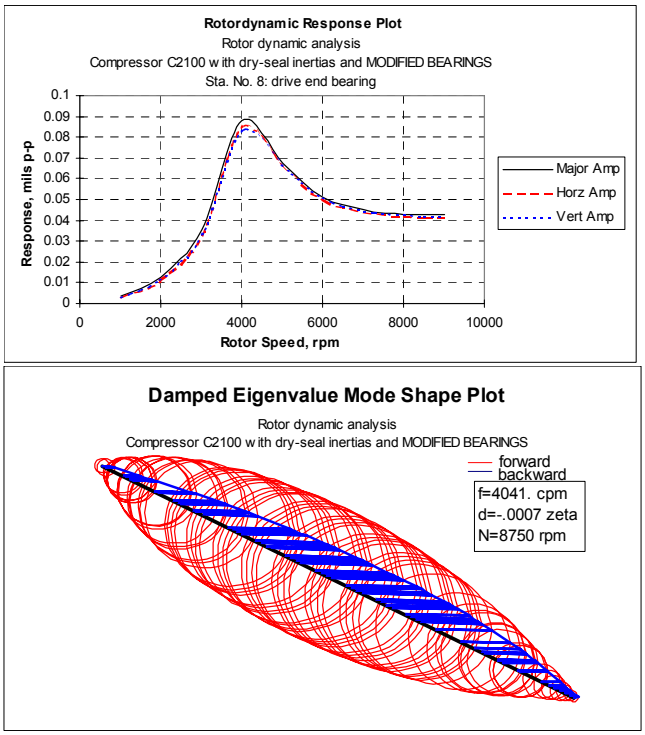

Figure 11: Imbalance Response of Compressor and Rotor Mode Shape at Top Speed.

The mode shape in Figure 11 shows that at the bearing locations the rotor motions are quite small while the vibration amplitude at the seal locations (rotor midspan) is much larger. The instability is certainly associated with a poor design and inadequate selection of the multiple-lobe bearings and the lockup of the oil seal rings.

Finally, Figure 12 shows the field recorded vibration spectra. The rotor speed is 7,860 rpm and the dangerously high amplitude subsynchronous vibration develops at a frequency of 59 Hz (3,532 rpm). Thus, the whirl ratio equals 0.45. The rotordynamic predictions are conservative!

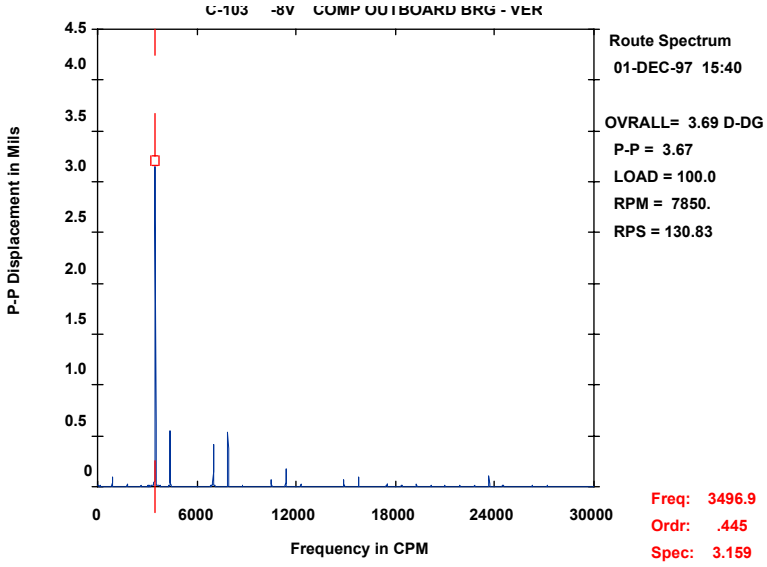

Figure 12: Field Vibration Spectrum Showing Rotordynamic Instability for Compressor Example.

The rotordynamics example demonstrates the importance of fluid film bearings and seals on the dynamic response of rotating machinery. In the example presented, the sudden onset of severe subsynchronous vibration with large amplitude brought an unexpected stop in operation of the unit with an enormous cost to the user, several hundred thousand of dollars per day over an undisclosed amount of time. Fortunately, current monitoring techniques enabled the engineers to prevent a catastrophic failure with a larger financial and human cost.

4.0 PUMP ROTORDYNAMICS

The rotordynamics of pumps is more complicated due to a distinctive number of operating features mostly load dependent; i.e. related to the power (pressure and flow conditions). The most important issues to consider in a realistic analysis are:

a) Pumps typically handle large density liquids and the effects of inter-stage and wear seals on the rotor-bearing system dynamics is most important. Liquid seals generate substantial direct stiffnesses and added mass coefficients that can change dramatically the natural frequencies (critical speeds) of a pump. Thus, there is a distinction between “dry” and “wet” critical speeds [4, 11].

b) Uneven static pressure distribution at the pump discharge volute generates a side radial load. This load, of importance in single-tongue volute casing pumps, is greatly affected by operation away from the pump Best Efficiency Point [12, 13]. The hydraulic load, whose magnitude and direction depends on operation away from BEP, causes the support bearings to become more or less loaded, thus affecting rotordynamic behaviour [14].

c) The rotating liquid flowing through the impellers causes a condition of *hydraulic imbalance* due to inaccuracies in the manufactured impeller surfaces. The hydraulic induced synchronous force is most difficult to predict and even worse to measure in the field [11].

d) Dynamic forces and moments arise due to changes in pressure within the small clearance between the pump casing and its shroud. Lateral and angular shaft motions induce this type of impeller-shroud excitation force (and moment) which can affect greatly the stability of high power density pumps; in particular in multiple-stage pumps which are quite flexible (low critical speeds) [15, 16].

The analysis of seal flow and the prediction of seal reaction forces will be considered in the third of these lectures [17]. A brief discussion on hydraulic forces and impeller-shroud interaction forcers follow.

4.1 Static Radial Loads on Centrifugal Pumps

There two formulas for estimation of the static radial load acting on a centrifugal pump, one from the Hydraulic Institute [12] and the other attributed to Stepanoff [13]. Both formulas are derived from extensive measurements. The two methods predict a minimum radial load near the best efficiency point (BEP). Radial loads increase as the flow increases or decreases from the BEP. The Hydraulic Institute (HI) method predicts radial loads increasing at a faster rate with deviations from the BEP % volumetric rate at higher specific speeds.

Figure 13 displays the load direction and its relative magnitude. From [12], at 0 % flow capacity the radial load vector peaks and lies along a line from the shaft center to the cutwater. As the flow increases, the load decreases and moves around the volute in a direction opposite to the shaft rotation. At the BEP the load direction is opposite to the line joining the shaft center and the cutwater. This trend continues as the volumetric capacity increases past 100%.

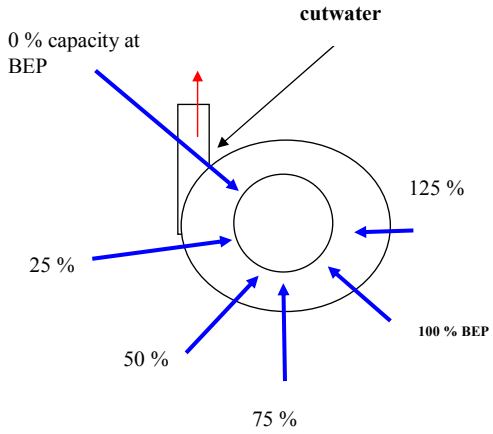

Figure 13: Direction of Radial Load on Single Volute Casing (Hydraulic Institute [12]).

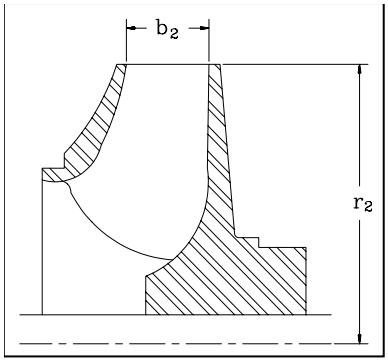

Typical pump impeller geometry, D_o=2 r_2

The formulae for estimation of a radial load (F_R) [lbf] in single volute pumps using the Hydraulic Institute method [12] (sub index $_H$) and Stepanoff method (sub index $_S$) [12, 13] are:

$$F_{RH} = K_H \rho g H D_o b$$
$$F_{RS} = K_S \rho g H D_o b \qquad (10)$$

The radial force depends on the fluid head (pressure rise) H, fluid density (ρ) at the pump exit, impeller outer diameter (D_o) and impeller discharge width including side plates(b). The HI load factor (K) varies with deviations from the BEP and specific speed (NS), see Figure 14. The HI [12] data reaches to 120% operating capacity. In Stepanoff's equation, the load factor K_S (empirically determined) is a function of the operating pump flow rate (Q) [13]:

$$K_S = 0.36\left[1 - \left(\frac{Q}{Q_{BEP}}\right)^2\right] \qquad (11)$$

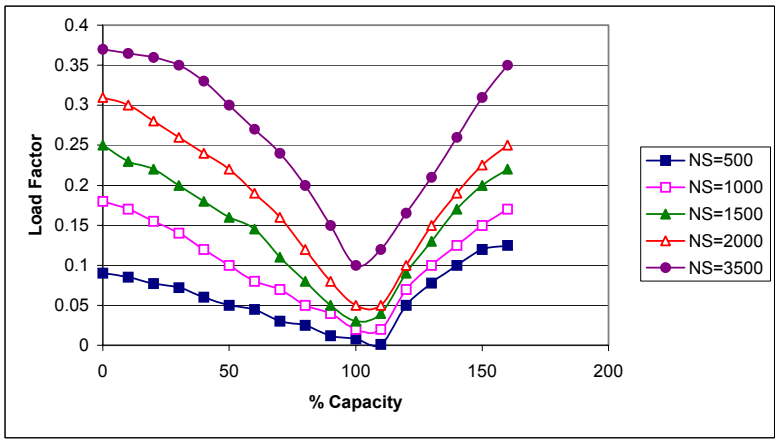

Figure 14: HI Load Factor *(K)* vs. Percent Flow Capacity for Several Specific Speeds [12].

Note that the magnitude of the radial load is proportional to the pumped fluid density as well as the pressure head. Figures 15 depict predicted hydraulic radial loads from both methods for a typical pump application. Stepanoff's method predicts loads about twice as large as those derived from the HI method! There is also a discrepancy on the predicted direction of load action. Although Stepanoff's method does not specify the direction of the hydraulic static load, experimental work by Moore et al. [18] on compressors evidences a load direction opposite to that given by the Hydraulic Institute.

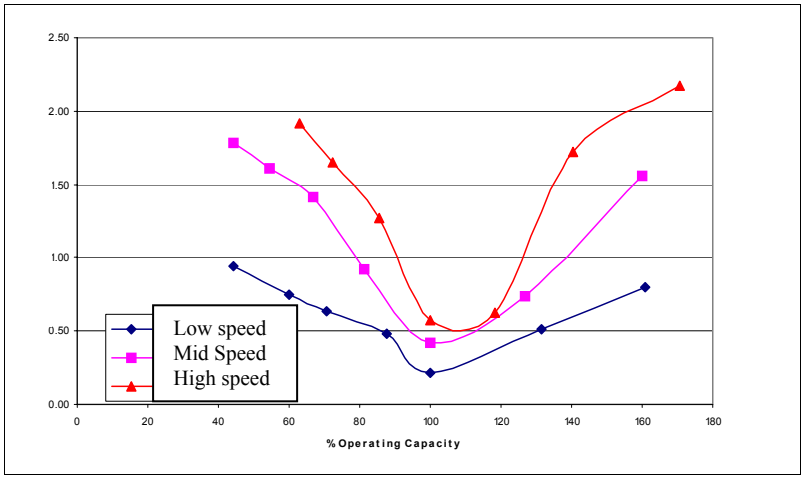

Figure 15a: Predicted Radial Loads using Hydraulic Institute Method [12].

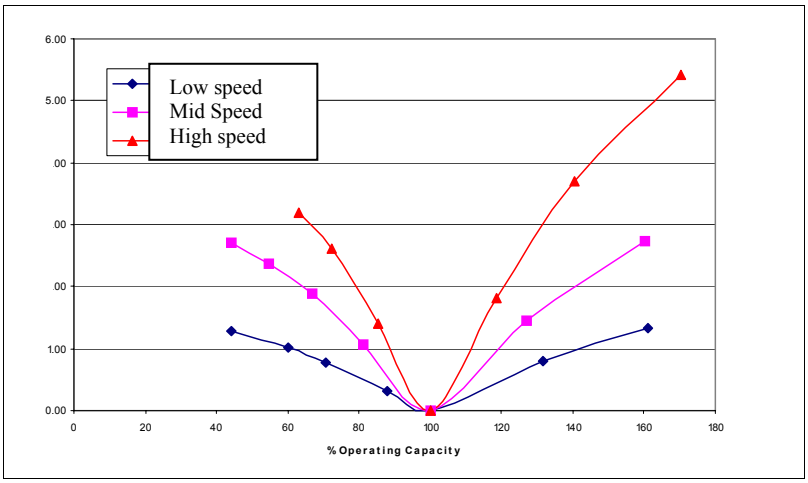

Figure15b: Predicted Radial Loads using Stepanoff Method [13].

Incidentally, radial loads are much reduced in pumps using a diffuser-casing or multiple-tongue volute-casing [12, 14].

4.1 Hydraulic Imbalance Force on Centrifugal Pumps

Unsteady flow conditions within the pump also generate time-varying forces. The most apparent force is that induced by the rotating fluid, i.e. a centrifugal load, synchronous with shaft speed, and exacerbated by the surface condition of the flow path within the pump impeller. The predicted hydraulic dynamic load, F_{imb}, relies on empirical test data [14] and follows the definition:

$$F_{imb} = K_{1X}\, \rho g H D_o b \qquad (12)$$

The dynamic hydraulic load is proportional to the fluid density, pressure discharge and the impeller geometry. Note that pump head is proportional to rotational speed^2 , $H \sim \Omega^2$; thus, as with mechanical imbalance, $F_{imb} \sim \Omega^2$. The empirical dynamic load factor (K_{1X}) is a function of the flow condition (Q/Q_{BEP}). As per Adams [14], "poor hydraulic design quality and poor impeller dimensional control, such as with cheap low-quality sand cast impellers, tends to yield large values of the parameter K_{1X}. Childs [14], from published test data, recommends for operation at BEP,

$$0.005 \le K_{1X} \le 0.015;\ 0.02 \le K_{1X} \le 0.12 \qquad (13)$$

for precision-cast and sand-cast impellers, respectively. Adams [14] lists values of the dynamic load factor (K) for other flow conditions and ratio of whirl speed to rotor speed.

Note that in practice, pump rotors well balanced mechanically within acceptable levels; in operation can still show significant levels of shaft synchronous motion. Attempting to improve this performance condition by mechanical means, i.e. by conducting further mechanical shop balancing, will be a futile effort unless the pump impellers are better designed and manufactured with a process ensuring high quality control of surfaces. Incidentally, all impellers after extended periods of operation will tend to degrade its mechanical imbalance (wear, tear, debris accumulation), thus also exacerbating the hydraulic imbalance force as flow surface conditions also degrade.

4.2 Impeller-Rotor Interaction Forces in Centrifugal Pumps

Childs [16] reviews cases of rotordynamic instability ascribed to impeller-rotor interaction forces in well designed high performance turbomachinery. The dynamic forces are largely determined by the lateral motions of the pump rotor, i.e. they depend on the rotor (radial and angular) displacement, velocity and acceleration and described adequately with conventional stiffness, damping and inertia matrices. As the rotor vibrates, the impeller moves and open/closes the secondary flow paths along the front shroud and back face of the impeller. The fluid flowing through these gaps is also displaced and a dynamic pressure field is generated thus creating the dynamic forces and moments acting on the rotor.

There is no definitive analysis on impeller –rotor interaction forces in pumps and compressors. For liquid pumps, predictive analysis relies on a handful of experimental results conducted at Cal Tech [19] and Sulzer [20]. To this date, the most important question is to pinpoint the exact source of the dynamic forces (or moments). The impeller-rotor interaction force combines the contributions of dynamic forces arising from the front and back faces of the impeller as well as those arising from the neck-ring seal and inter-stage seals. Impeller lateral forces are typically modelled as

$$\begin{bmatrix} F_X \\ F_Y \end{bmatrix} = -\begin{bmatrix} K_D & K_C \\ -K_C & K_D \end{bmatrix}_I \begin{Bmatrix} X \\ Y \end{Bmatrix} - \begin{bmatrix} C_D & C_C \\ -C_C & C_D \end{bmatrix}_I \begin{Bmatrix} \dot{X} \\ \dot{Y} \end{Bmatrix} - \begin{bmatrix} M_D & M_C \\ -M_C & M_D \end{bmatrix}_I \begin{Bmatrix} \ddot{X} \\ \ddot{Y} \end{Bmatrix} \qquad (14)$$

where the D and C sub-indices denote direct and cross-coupled coefficients, respectively. This reduced model force representation assumes rotational symmetry and circular centered orbital motions. Test results are typically presented in dimensionless form as

$$\overline{K}_D, \overline{K}_C = \frac{K_D, K_C}{m_{.ref}\, \Omega^2};\quad \overline{C}_D, \overline{C}_C = \frac{C_D, C_C}{m_{.ref}\, \Omega};\ \overline{M}_D, \overline{M}_C = \frac{C_D, C_C}{m_{.ref}};\ m_{ref} = \pi \rho \left(\frac{D_o}{2}\right)^2 b_2 \qquad (15)$$

with Ω as the pump speed and m_{ref} as a reference fluid mass. The magnitude of the reference mass is large since it relates to a volume of a solid disk of diameter D_o and thickness b_2. If M_c~0, the whirl frequency ratio, $WFR=K_c/(C_D\Omega)$, relates the whirl frequency of unstable motions to shaft speed. A WFR=0.5 means that the pump cannot operate stable at a speed above two times (=1/WFR) the system first natural frequency. Table 6 presents the dimensionless force coefficients given in the literature and Figure 16 displays the four pump impellers tested at Sulzer [20]. These tests as of particular importance since the clearance between the impeller shroud and casing are small, 0.067 to 0.081 mm, and representative of actual applications.

Table 6: Impeller Force Coefficients from Test Data. Sources [14, 16]

	$\overline{K}_D$	$\overline{K}_C$	$\overline{C}_D$	$\overline{C}_C$	$\overline{M}_D$	$\overline{M}_C$	WFR	Note
CT-volute	-2.5	1.10	3.14	7.91	6.51	-0.58	0.35	Φ=0.092
CT-diffuser	-2.65	1.04	3.80	8.96	6.60	-0.90	0.27	Φ=0.092
Radial flow impeller	-0.42	-0.09	1.08	1.88	1.86	-0.27	-	BEP, vaneless diffuser
S-Diffuser (2)	-5.0	4.4	4.2	17.0	12.0	3.5	1.05	2 krpm
S-Diffuser (4)	-2.0	7.5	4.2	8.5	7.5	2.0	1.78	4 krpm
S_ with swirl brake	-2.2	7.7	3.4	8.6	6.7	3.1	2.26	4 krpm, BEP, Type D
S- with face seal	-4.2	5.1	4.6	13.5	11.0	4.0	1.11	BEP, Type A

S- Sulzer test data (small clearance); CT: Cal Tech test data, $\Phi = 2Q/\left(\pi b_2 D_o^2 \Omega\right)$ flow coefficient

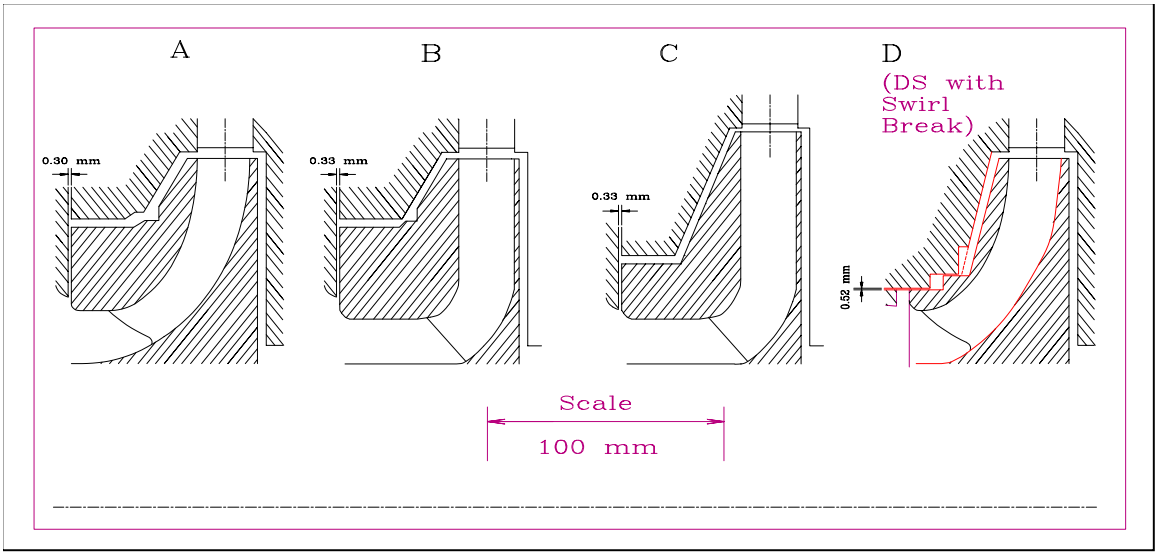

Figure 16: Tested Impellers at Sulzer [20].

From the experimental results, the following conclusions are derived

- Impellers have negative direct stiffness and large direct and cross-coupled inertia coefficients.
- The cross coupled stiffnesses are much larger for tight clearance impellers thus generating large destabilizing forces at rotor speeds below the rotor-bearing system critical speed, i.e. $WFRs > 1$.

- The shroud generates most of the destabilizing forces in a pump impeller [16].
- Enlarged clearance in neck ring seals aggravate the generation of cross-coupled forces since the swirl flow into the seal increases. Enlarged clearances are the result of transient rub events in operation of a pump.
- At reduced flow rates ($< Q_{BEP}$), the impeller cross-coupled stiffnesses are lower.
- Impeller-volute interaction forces are small and benign [16].
- In a radial flow impeller cross-coupled stiffnesses are small, i.e. the destabilizing force is negligible since the projected axial area of the shroud is quite small.

Childs has advanced two bulk-flow analyses [21, 22] for the prediction of impeller-interaction forces in pumps and compressors, respectively. The first analysis considers the secondary flow through a pump impeller shroud and derives dynamic force coefficients as a function of the operating condition and whirl frequency ratio. Comparison of predictions to Sulzer's test data is good for the whirl frequency ratio and reasonable for cross-coupled stiffness and direct damping. Predictions of other coefficients are rather poor. Note that the bulk-flow model, by integrating the velocity film across the thin film clearance, cannot reproduce regions of flow recirculation. CFD studies demonstrate these flow zones extend over the entire secondary flow path, in particular when tight exit seals are in place.

Childs concludes that leakage flowing radially inward towards the neck ring seals generates a large inlet swirl, i.e. mean circumferential flow larger than 50% of rotor surface speed, which generates large cross-coupled stiffnesses able to induce rotordynamic instability, i.e. reduce stability margin. Childs [16] states that the impeller-rotor interaction forces increase sharply with decreasing clearance between the impeller shroud and the pump housing. Ehrich [15] states that enlarged clearances in the exit seal due to wear or damage will increase the circumferential flow velocity over the shroud and into the seal, thus enlarging the cross-coupled forces [15].

In the most recent analysis [21], Childs performs a complete bulk-gas flow analysis integrating the secondary flows through the front shroud and its neck-ring seal, as well as the leakage (inward or outward) flow through the impeller back face and the inter stage seal. The predictions, applicable to pumps, are in agreement with test data for moment coefficients when using unrealistic values for the inlet losses into the eye lacking labyrinth seals. Other predictions for a compressor stage are reasonable; albeit showing "fluidic" resonances at low whirl frequency ratios. In [21], individual forces from each element are calculated. The authors find that the eye seal and interstage seals account for 80% and 18% of the cross-coupled stiffness, while the front shroud contributes with just 2.2%. The effect of the back shroud is entirely negligible, even for radial inflow. Thus, the impeller-rotor interaction forces in compressors appear to be mostly affected by the seals.

Industry uses the API standard Wachel-formula [16] to predict the aerodynamic cross-coupled force in a compressor. The results in [21] show more conservative results, i.e. less destabilizing forces, than the accepted formula. However, there have been instances when compressors have become unstable in spite of their design with consideration of Wachel's aerodynamic force. Childs [21] concludes that the deficiency in predictive analysis properly validated by experimental results remains. Impeller induced forces are thought as the "last" great unknown in modern rotordynamics.

4.3 Example of Pump Rotordynamics Analysis

A linear rotordynamics analysis for an 11-stage pump follows. Figure 17 depicts the rotor structural model. The pump rotor weighs 363 lb and its length is 97.45 inch. The shaft mean diameter at the impeller locations is 2.5 inch in and the bearing span is 79.4 inch. The impellers are 8.12 inch in diameter (D_o) with a throat discharge width (b_2) of 0.36 inch. The liquid density is 1.5 slug/ft^3 (775 kg/m^3).

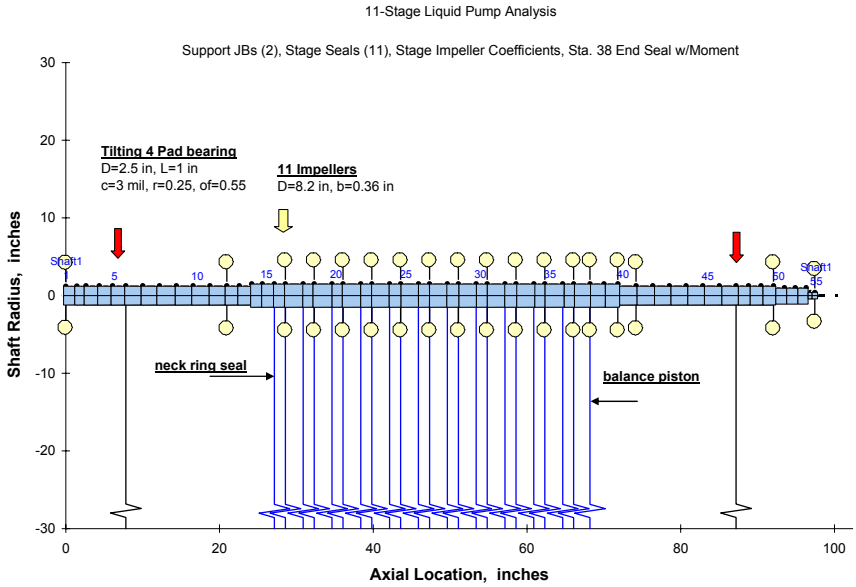

Figure 17: Rotordynamics Model of 11-Stage Pump.

Two identical four-tilting pad bearings support the pump. The bearing diameter and length equal 2.5 inch and 1.0 inch, respectively, and the radial clearance is 0.003 inch (76 micron). Each pad arc is 80° with pivot offset and assembly preload equal to 0.55 and 0.25, respectively. The lubricant viscosity and specific gravity are 2 micro-Reyns (13.8 cPoise) and 0.85. Each bearing supports half the rotor weight (Load between pad configuration).

Bearing and impeller seal force coefficients are calculated with XLTRC^2 software suite based on the analyses in [22] and [23]. Impeller force coefficients are estimated from tabular results based on the Sulzer experimental findings, see Table 6, ref.[16], for operation at Best Efficiency Point.

In the rotor model, there are 2 bearing stations (6, 47); 12-seal stations (16, 18, 20, 22, 24, 26, 28, 30, 32, 34, 36, end seal 38); and 11-impeller stations (17, 19, 21, 23, 25, 27, 29, 31, 33, 35, 37).

The rotor is rather flexible. The first two free-free modes are at just 2,346 rpm and 5,469 rpm as shown in Figure 18.

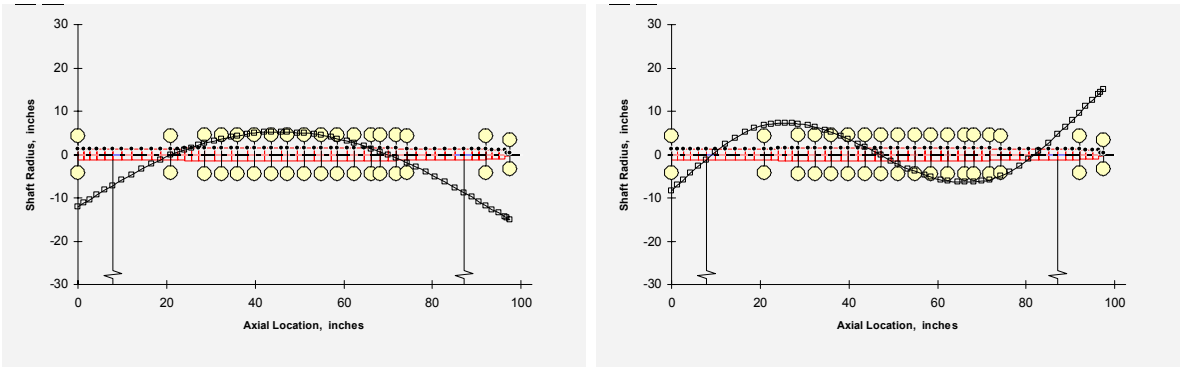

2,346 rpm **5,469 rpm**

Figure 18: Free-Free (Undamped) Modes of Multi-Stage Pump.

The eigenvalue analysis predicts the damped natural frequencies, damping ratios and critical speeds for a range of pump rotational speeds. Table 7 summarizes the predictions for the "dry" and "wet" conditions. The dry condition only accounts for the tilting pad bearing force coefficients. The wet case includes the effects of the bearings, seals and impellers on the pump rotordynamics.

Table 7: Critical Speeds, Natural Frequencies and Damping Ratios for Multiple Stage Pump – DRY Condition

DRY			mode		Forward modes		mode
Critical speeds	cpm	damp ratio	number	Speed	damp ratio	cpm	number
	1340	0.007	2	3500 rpm	0.007	1340	2
	5155	0.013	8		0.013	5140	8

WET			mode		Forward modes		mode
Critical speeds	cpm	damp ratio	number	Speed 3500 rpm	damp ratio	cpm	number
	400	-0.024	2		-0.169	716	2
	1482	0.023	4		-0.010	1451	4
	3574	0.026	10		0.026	3574	10
					0.010	11340	12

For the "dry" condition, the rotor will traverse two lightly damped critical speeds (1340 & 5155 rpm) in the speed range from 1000 to 6000 rpm. Figure 19 depicts the map of damped natural frequencies and damping ratios versus shaft speed for the forward whirl modes. The rotor modes at the design speed of 3,500 rpm are also depicted in the Figure.

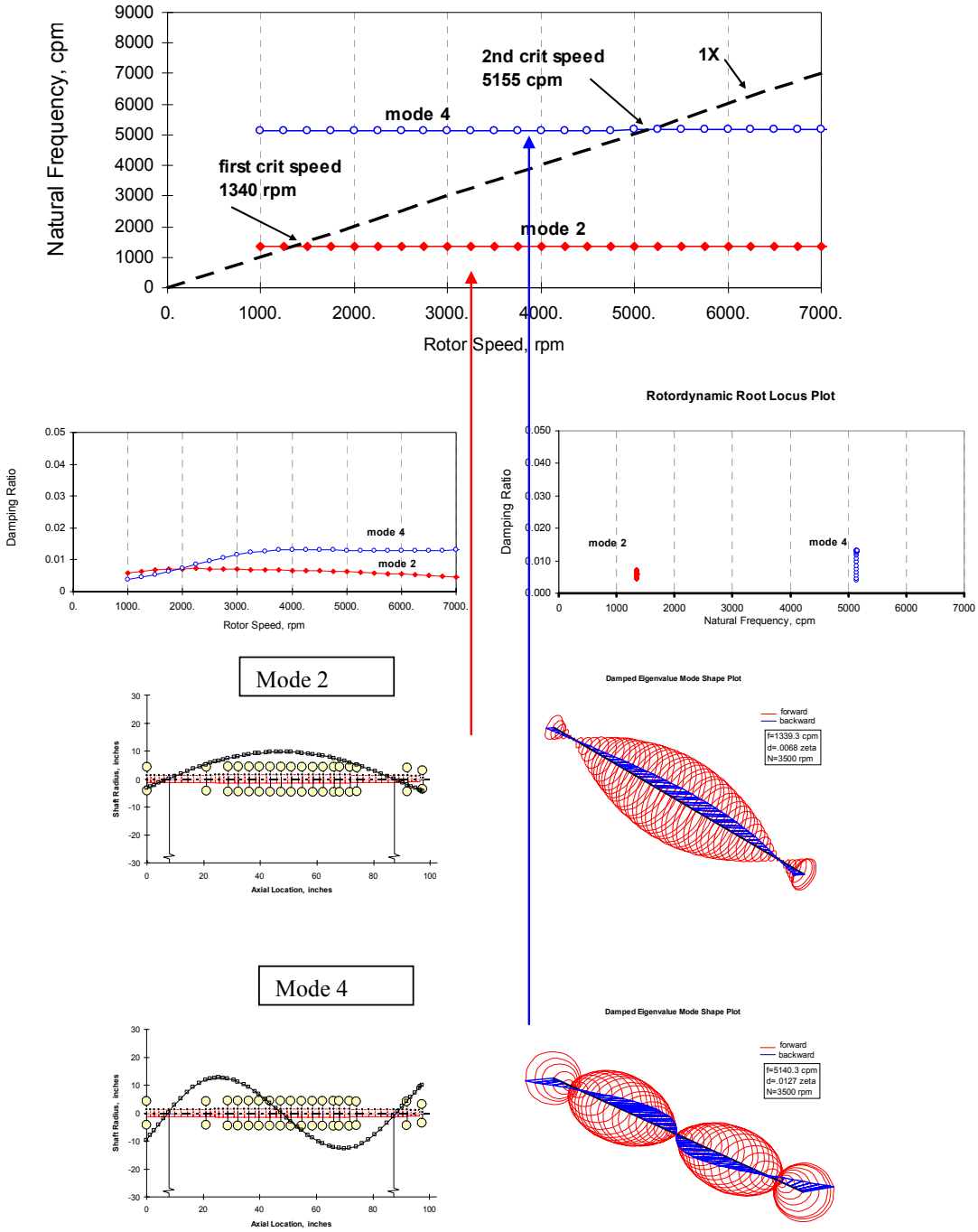

Figure 19: Natural Frequencies, Damping Ratios and Mode Shapes for Pump - DRY Case, Forward Whirl Damped Mode Shapes at Operating Speed (3,500 rpm).

Note that the rotor mode shapes are rather flexible with nodes at the bearing locations, hence the small damping ratios. Figure 20 shows the damped natural frequencies and mode shapes for the "wet" condition. Note that the critical speeds have "dropped" substantially due to the seals mainly. Furthermore, the damping ratios are negative for most of the operating speed range. The multiple stage pump will be unstable nearly from start up conditions.

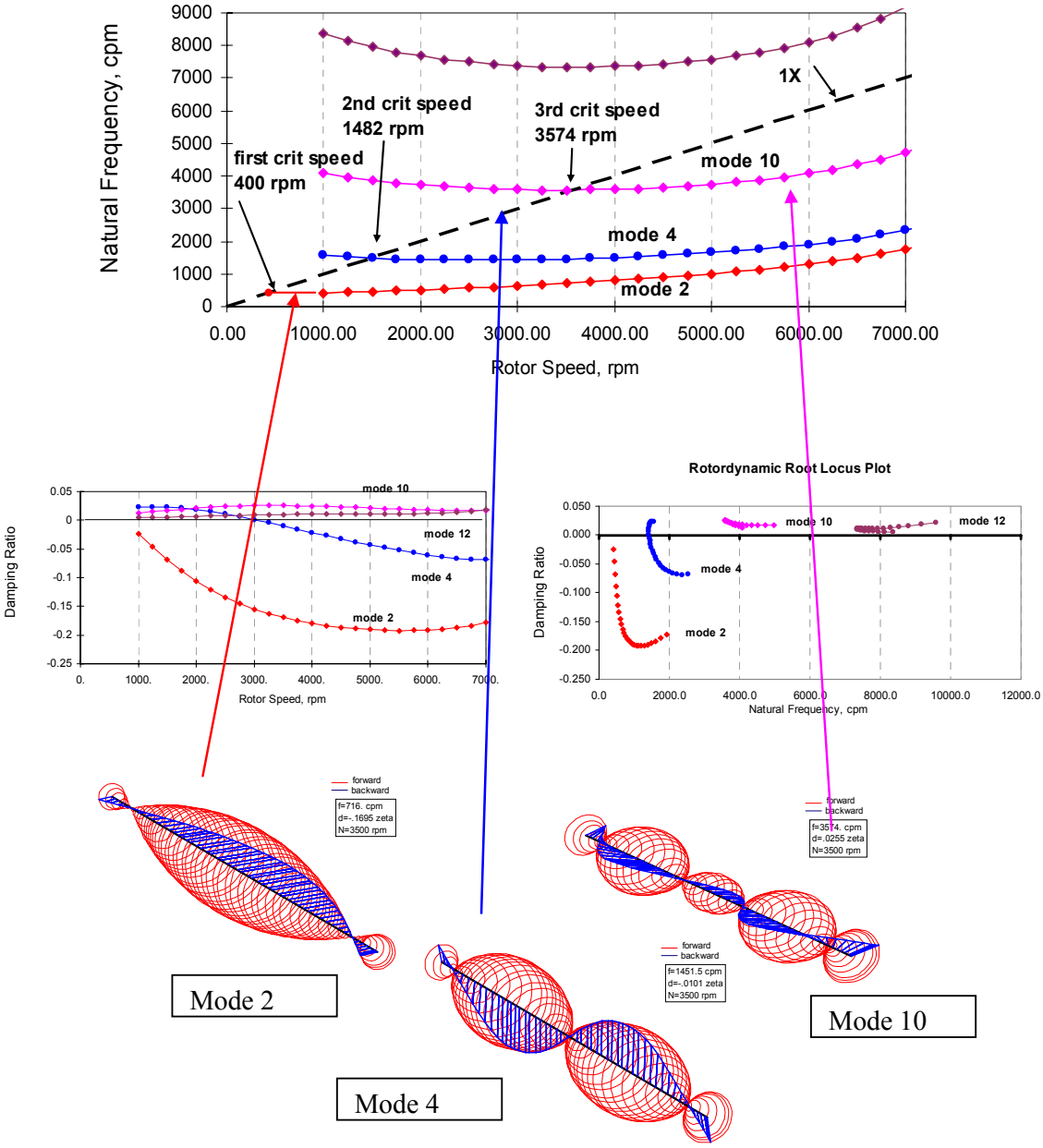

Figure 20: Natural Frequencies, Damping Ratios and Mode Shapes for Pump - WET Case, Forward Whirl Damped Mode Shapes at Operating Speed (3,500 rpm).

4.4 Closure

Synchronous response analysis is not conducted since the pump is unstable for nearly all shaft speeds. The rotordynamics predictions evidence the need to redesign the pump. The recommendations to follow are:

- Increase shaft diameter to make rotor more rigid thus raising (free-free mode) natural frequencies.
- Decrease bearing span to allow for more shaft motions at the bearing locations (avoid location of bearings at nodal points).
- Add inlet-anti swirl brakes into neck ring seals to reduce development of circumferential flow speed and ameliorate generation of cross-coupled destabilizing forces. Add shunt injection on balance piston.

- Verify predictions for impeller-interaction forces. Use latest test data if available.
- Re-design oil-lubricated bearings. Current configuration shows too large stiffness and too much damping. Enlarge slightly the clearances if applicable.

The following two lectures provide the fundamentals of fluid film bearing and seal design and their effect on the rotordynamics of turbomachinery. The importance of fluid inertia and flow turbulence on modern bearing and seal configurations is detailed along with applications to a cryogenic liquid turbopump.

REFERENCES

[1] Self-Excited Vibrations in High-Performance Turbomachinery, F. Ehrich & D. Childs, Mechanical Engineering, **106**, 5, pp. 66-79, May 1984.

[2] Introduction to Modern Lubrication, L. San Andrés, Lecture Notes (#1) in Modern Lubrication, http://phn.tamu.edu/TRIBGroup, 2002.

[3] Design and Application of Squeeze Film Dampers in Rotating Machinery, F. Zeidan, L. San Andrés & J. Vance, Proc. of the 25th Turbomachinery Symposium, TAMU, pp. 169-188, 1996.

[4] Turbomachinery Rotordynamics, (chapter 4), D. Childs, John Wiley & Sons, Inc., 1993.

[5] Annular Gas Seals and Rotordynamics of Compressors and Turbines, D. Childs & J. Vance, Proc. Of the 26th Turbomachinery Symposium, TAMU, pp. 201-220, 1997.

[6] Gas Damper Seal Test Results, Theoretical Correlation, and Applications in Design of High-Pressure Compressors, P. De Choudhury, F. Kushner & J. Li, Proc. Of the 29th Turbomachinery Symposium, TAMU, 2001.

[7] XLTRC^2 Rotordynamics Software Suite, Turbomachinery Laboratory, Texas A&M University, 2002.

[8] A Finite Rotating Shaft Element Using Timoshenko Beam Theory, H.D. Nelson, ASME Journal of Mechanical Design, **102,** pp. 793-803, 1980.

[9] Transient Analysis of Rotor-Bearing System Using Component Mode Synthesis, H.D. Nelson & H. Meacham, ASME Paper 81-GT-10, Gas Turbine Conference.

[10] A Virtual Tool for Prediction of Turbocharger Nonlinear Dynamic Response: Validation Against Test Data, L. San Andrés, L., J.C. Rivadeneira, K. Gjika, C. Groves, and G. LaRue, ASME Paper GT 2006-90873, 2006.

[11] Pump Rotordynamics made Simple, M. Carbo & S. Malanoski, Proc. Of the 15th International Pump Users Symposium, TAMU, pp. 167-203, 1998.

[12] Hydraulic Institute Centrifugal Pump Design and Application, pp. 103-105, 1994.

[13] Stepanoff, A. J. "Centrifugal and Axial Flow Pumps-Theory, Design, and Application," 2nd Edition, Wiley, New York, NY. 1957.

[14] Rotating Machinery Vibration, (Chapter 6), M. Adams, M. Dekker, Inc., 2001.

[15] Handbook of Rotordynamics, F. Ehrich, Mc-Graw-Hill Co., 1992.

[16] Turbomachinery Rotordynamics, (chapter 6), D. Childs, John Wiley & Sons, Inc., 1993.

[17] Annular Pressure Seals and Hydrostatic Bearings, L. San Andrés, Design and Analysis of High Speed Pumps, Von Karman Institute for Fluid Dynamics, Lecture Series, March 2006.

[18] Aerodynamically Induced Radial Forces in a Centrifugal Gas Compressor - Part 1: Experimental Measurement, J. Moore & M. Flathers, ASME Paper 96-GT-120, 1996.

[19] Experimental Measurements of Hydrodynamic Stiffness Matrices for a Centrifugal Pump Impeller, D. Chamieh, A.J. Acosta, T.K. Caughey & R. Franz, Proc. Of the Workshop in Rotordynamics Instability Problems in High Performance Turbomachinery, TAMU, NASA CP-2250, pp. 382-398, 1982.

[20] Measurement of Hydrodynamic Matrices of Boiler Feed Pump Impellers, U. Bolleter, A. Wyss, I. Welte & R. Struchler, ASME Journal of Vibrations, Acoustics, Stress reliability and Design, **109**, 1987.

[21] Rotordynamic Stability predictions for Centrifugal Compressors Using a Bulk-Flow Model to Predict Impeller Shroud Force and Moment Coefficients, M. Gupta & D. Childs, ASME Paper GT2006-90374, 2006.

[22] Turbulent Flow, Flexure-Pivot Hybrid Bearings for Cryogenic Applications, L. San Andrés, ASME Journal of Tribology, Vol. 118, 1, pp. 190-200, 1996.

[23] Effect of Shaft Misalignment on the Dynamic Force Response of Annular Pressure Seals, L. San Andrés, STLE Tribology Transactions, Vol. 36, 2, pp. 173-182, 1993.